RSC Advances

PAPER

Cite this: *RSC Adv.*, 2016, **6**, 105406

Catalytic performance of layered double hydroxide nanosheets toward phenol hydroxylation†

Guoqing Cui, Fei Wang, Shan He* and Min Wei*

Received 26th July 2016
Accepted 28th October 2016

DOI: 10.1039/c6ra18917b

www.rsc.org/advances

Layered double hydroxides (LDHs) materials have shown promising behaviour in heterogeneous catalysis, and increasing the amount of exposed active sites is crucial to enhance their catalytic performance. In this work, CuMgAl-LDH@mSiO$_2$ nanosheets were prepared by delaminating the CuMgAl(NO$_3$)-LDH microcrystals followed by coating a layer of SiO$_2$. Structural characterizations based on SEM and BET display their slice morphology with average thickness of 5.2 nm and a large specific surface area of 244.3 m^2 g^{-1}. This gives rise to excellent catalytic performance toward phenol hydroxylation (conversion: 45.6%; selectivity: 97.3%). Especially, the normalized activity value is as high as 330.8 (mol phenol/mol Cu^{2+}) with the efficiency of peroxide up to 91.1%. This is, to the best of our knowledge, the highest value for Cu-based heterogeneous catalysts in this reaction. This work demonstrates the unique structural feature of CuMgAl-LDH@mSiO$_2$ nanosheets with efficient exposure of active sites and its remarkably enhanced catalytic activity toward phenol hydroxylation.

1. Introduction

Hydroxylation of phenol with hydrogen peroxide is an important industrial reaction to produce catechol (Cat) and hydroquinone (HQ), which are promising intermediates for fine chemicals (perfumes, pharmaceuticals, pigments and pesticides).[1–4] Traditionally, homogeneous catalysts (*e.g.*, soluble metal salts[5] and inorganic acids[6,7]) are commonly used in this reaction with rather good activity and selectivity, but the difficulties in catalyst separation/recyclability restrict their practical applications. Great efforts have recently been focused on the exploration of heterogeneous catalysts (*e.g.*, zeolite-encapsulated metal[8,9] complexes and metal oxides[10]), which are suitable for separation but suffer from low catalytic activity. In spite of the great progress achieved, how to design and prepare desirable catalysts with the merits of satisfactory catalytic performance and facile manipulation remains a challenge.

Layered double hydroxides (LDHs), a class of two dimensional layered materials generally expressed by the formula $[M_{1-x}^{2+}M_x^{3+}(OH)_2]^{x+}(A_{x/n}^{n-})^{x-}\cdot mH_2O$ (M^{2+} and M^{3+} represent di- and tri-valent metal cations, respectively; A^{n-} is a *n*-valent anion), have attracted an increasing attention in the field of heterogeneous catalysis due to their versatility in chemical composition and architectural morphology.[11–13] More importantly, LDHs microcrystals can be exfoliated into monolayer nanosheets, which are widely used as building blocks for the fabrication of photo- or electric-functional materials.[14–16] It has been reported that Cu-containing LDHs show good catalytic performance toward phenol hydroxylation, based on the activated adsorption of reactant upon Cu^{2+} site.[17–20] This inspires us to synthesize Cu-containing LDHs nanosheets *via* delamination and to evaluate the catalytic behavior in phenol hydroxylation. If all the active Cu^{2+} ions are located in the exterior surface and participate in the catalytic reaction, an extremely high activity and efficient use of hydrogen peroxide would be obtained.

Herein, we report CuMgAl-LDH@mSiO$_2$ nanosheets *via* delamination of LDH microcrystals followed by deposition of a mesoporous SiO$_2$ coating (Scheme 1), and investigate their catalytic performance toward phenol hydroxylation. The resulting CuMgAl-LDH@mSiO$_2$ nanosheets show a uniform morphology, with an average thickness of 5.2 nm and specific surface area of 244.3 m^2 g^{-1}. The nanosheets catalyst displays an enhanced catalytic activity along with the decrease in the sheet thickness, and the monolayer sample exhibits the best catalytic performance (conversion: 45.6%; selectivity: 97.3%). Notably, the normalized activity of 330.8 (mol phenol/mol Cu^{2+}) and peroxide efficiency of 91.1% are simultaneously obtained, which is to our knowledge the highest among the identical reaction conditions for Cu-based heterogeneous catalysts. In

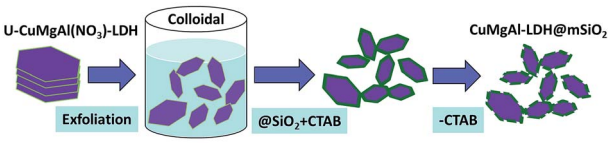

Scheme 1 Schematic synthesis of the CuMgAl-LDH@mSiO$_2$ process.

State Key Laboratory of Chemical Resource Engineering, Beijing University of Chemical Technology, Box 98, Beijing 100029, P. R. China. E-mail: vh30@163.com; weimin@mail.buct.edu.cn; Fax: +86-10-6442-5385

† Electronic supplementary information (ESI) available. See DOI: 10.1039/c6ra18917b

addition, the SiO_2 coating prevents the aggregation of highly-active LDH nanosheets, and its porous structure enables the diffusion/transport of reactants, accounting for the catalytic stability and recyclability. Our approach holds significant promise for the design and preparation of an ultrafine, highly-active CuMgAl-LDH nanocatalyst, which can serve as a promising candidate in phenol hydroxylation reaction.

2. Experimental section

2.1 Materials

The following analytical-grade inorganic chemicals were purchased from Sigma-Aldrich and used without further purification: NaOH, Na_2CO_3, $Cu(NO_3)_2\cdot 3H_2O$, $Mg(NO_3)_2\cdot 6H_2O$, $Al(NO_3)_3\cdot 9H_2O$, $NaNO_3$, H_2O_2 (30% mass), tetraethyl orthosilicate (TEOS), hexadecyl trimethyl ammonium bromide (CTAB), phenol, pyrocatechol, hydroquinone and *p*-benzoquinone. Deionized water without carbon dioxide was used in all the experimental processes.

2.2 Synthesis of CuMgAl-LDH@mSiO$_2$

2.2.1 Synthesis of carbonate-containing CuMgAl-LDH microcrystals. CuMgAl-LDH microcrystals were prepared by the urea decomposition method.[21] In a typical procedure, $Cu(NO_3)_2\cdot 3H_2O$, $Mg(NO_3)_2\cdot 6H_2O$ and $Al(NO_3)_3\cdot 9H_2O$ with a given molar ratio of $Cu^{2+}:Mg^{2+}:Al^{3+} = 3:37:20$ were dissolved in deionized water (200 ml) to give a solution with a total cationic concentration of 0.6 M (solution A). 0.33 mol of urea (CON_2H_4) was dissolved in water (200 ml) to obtain a base solution (solution B). Solution A and solution B were then mixed together by ultrasonic wave and stirring method. The resulting suspension was aged in a sealed Teflon autoclave at 120 °C for 24 h, washed thoroughly with water *via* centrifugation and then dried in an oven at 60 °C overnight. The CuMgAl-LDH precursor was labeled as U-CuMgAl(CO_3)-LDH.

2.2.2 Synthesis of nitrate-containing CuMgAl-LDH microcrystals. The CuMgAl(NO_3)-LDH microcrystals were prepared by a so-called salt–acid method.[22,23] U-CuMgAl(CO_3)-LDH (1.0 g) and sodium nitrate (127.0 g) were dissolved in deionized water (100 ml) in nitrogen atmosphere with stirring for 24 h, followed by addition of concentrated nitric acid (0.0045 mol) in the first hour. The resulting U-CuMgAl(NO_3)-LDH sample was centrifuged, washed and dried.

2.2.3 Synthesis of CuMgAl-LDH@mSiO$_2$. Delamination of U-CuMgAl(NO_3)-LDH sample (1.0 g) was carried out in formamide (400 ml) with vigorous stirring in nitrogen atmosphere for 24 h.[21,24] Afterwards, ethanol (100 ml), deionized water (25 ml), cetyl trimethyl ammonium bromide (CTAB, 0.6 g) and tetraethyl orthosilicate (TEOS, 0.9 ml) were added to the above suspension with stirring for 6 h. The resulting precipitate was washed with water *via* centrifugation and then dried in an oven at 60 °C overnight. Finally, 1.0 g sample of the resulting CuMgAl-LDHs nanosheets coated by a porous SiO_2 layer was dispersed in acetone (200 ml), refluxed at 56 °C heated by a water bath at 85 °C for 24 h to remove CTAB, followed by washing with ethanol and drying at 60 °C overnight (denoted as CuMgAl-LDH@mSiO$_2$). Elemental analysis and FT-IR spectroscopy were used to confirm the removal of surface CTAB. The amount of carbon element decreases markedly from 7.68% to 3.10% after the refluxing treatment, which is attributed to the elimination of CTAB. FT-IR spectrum (Fig. S1†) of CuMgAl-LDH@mSiO$_2$ before refluxing shows two bands in the region 2800–3000 cm^{-1} due to the vibrations of $-CH_2$ in CTAB, which disappear after refluxing in acetone.

2.3 Synthesis of CuMgAl-LDH nanoparticles as control samples

CuMgAl-LDH nanoparticles as control samples were synthesized by the separate nucleation and aging steps (SNAS) route developed by our group.[25] Typically, $Cu(NO_3)_2\cdot 3H_2O$, $Mg(NO_3)_2\cdot 6H_2O$ and $Al(NO_3)_3\cdot 9H_2O$ with a certain molar ratio of $Cu^{2+}:Mg^{2+}:Al^{3+} = 3:17:10$ were dissolved in deionized water (100 ml) to give a solution with a total cationic concentration of 0.09 M (solution A). NaOH and Na_2CO_3 were dissolved in deionized water (100 ml) with $[{CO_3}^{2-}] = 2.0\,[M^{3+}]$ and $[OH^-] = 1.8\,([M^{2+}] + [M^{3+}])$ (solution B). Solution A and solution B were then mixed in a colloid mill rotating at a steady rate of 3000 rpm for 2 min. The resulting suspension was aged in a sealed Teflon autoclave at 80 °C for 6 h. The obtained precipitate was washed thoroughly with water and dried in an oven at 60 °C overnight (denoted as S-CuMgAl-LDH-80). Similarly, the CuMgAl-LDH nanoparticle samples at aging temperature of 100 °C and 120 °C were also synthesized by the above-mentioned process (denoted as S-CuMgAl-LDH-100 and S-CuMgAl-LDH-120).

2.4 Characterization of samples

Powder X-ray diffraction patterns of the LDHs microsphere samples were performed on a Rigaku XRD-6000 diffractometer by use of Cu Kα radiation ($\lambda = 0.15418$ nm) at 40 kV and 40 MA, with a scanning rate of 10° min^{-1} and a 2θ angle scan range between 3° and 70°. The morphology of the samples was investigated using a scanning electron microscope (SEM; Zeiss Supra 55) with an accelerating voltage of 20 kV combined with energy-dispersive X-ray spectroscopy (EDX) for the determination of the metal composition. Transmission electron microscopy (HRTEM) images were recorded with JEOL JEM-2100-115 high-resolution transmission electron microscopes. The accelerating voltage was 200 kV in each case. The specific surface area measurements were performed on the basis of the Brunauer–Emmett–Teller (BET) method using a Quantachrome Autosorb-1C-VP analyzer.

2.5 Evaluation of catalytic performance

For the reaction of phenol hydroxylation, the catalyst (0.1 g) and phenol (1.0 g) were added successively to a boiling flask-3-neck containing deionized water (10 ml) equipped with a stirring bar and a thermostat. The reaction was initiated by adding H_2O_2 with a molar ratio of phenol : $H_2O_2 = 2:1$ at 65 °C for 1 h. The reaction product was analyzed off-line by a gas chromatograph (GC, Shimadzu, 2014C) equipped with a flame ionization detector (FID) and a PEG-20 M capillary column (0.25 mm in diameter, 30 m in length). The product analysis and calculation

were performed by an external standard method based on GC profile of the product mixture (Fig. S2†).

3. Results and discussion

3.1 Structural and morphological characterization

The XRD pattern (Fig. 1A, curve a) of the obtained U-CuMgAl(CO_3)-LDH sample displays a range of typical diffraction peaks at 2θ 11.7°, 23.5°, 34.9°, 39.5°, 47.0°, 60.9° and 62.3°, which are indexed to the (003), (006), (012), (015), (018), (110) and (113) of a CO_3^{2-}-containing LDH phase, respectively.[21] No other crystalline phase is detected, indicating the high purity of the sample. The delamination of NO_3^--containing LDH is much easier than CO_3^{2-}-containing LDH due to its weaker host–guest interaction.[21] For this reason, the interlayer CO_3^{2-} was replaced by NO_3^- *via* an ion exchange process. The resulting U-CuMgAl(NO_3)-LDH shows a (003) reflection at 2θ 10.8° (Fig. 1A, curve b), demonstrating an enlarged interlayer distance from carbonate phase (d_{003} = 7.48 Å) to nitrate phase (d_{003} = 8.93 Å). Finally, the sample of U-CuMgAl(NO_3)-LDH was delaminated to nanosheets coated with a SiO_2 layer (Scheme 1). In the case of CuMgAl-LDH@mSiO_2 sample (Fig. 1A, curve c), all the characteristic reflections of CuMgAl-LDH phase are not observed, indicating the LDH microcrystals have been peeled into thin slices without long-range ordered stacking.[21] No reflection of SiO_2 is detected, implying its amorphous state. For three control samples (S-CuMgAl-LDH-80, S-CuMgAl-LDH-100 and S-CuMgAl-LDH-120), they were prepared at different aging temperature for the purpose of tuning particle size. Their XRD patterns (Fig. 1B) show characteristic reflections of a carbonate-LDH phase, with much larger FWHM (Full Wave at Half Maximum) compared with U-CuMgAl(CO_3)-LDH sample, indicating lower crystallinity without the assistance of urea during the synthesis process. The particle size based on Debye–Scherrer equation is calculated to be 21.9 nm, 27.7 nm and 36.1 nm for S-CuMgAl-LDH-80, S-CuMgAl-LDH-100 and S-CuMgAl-LDH-120, respectively. The higher aging temperature leads to the larger particle size, accounting for the decreased FWHM and enhanced crystallinity.[26,27]

SEM images of these samples are shown in Fig. 2. U-CuMgAl(CO_3)-LDH (Fig. 2A) and U-CuMgAl(NO_3)-LDH (Fig. 2B) prepared by carbamide route display hexagonal plate-like microcrystals, with rather close mean particle size of 2.60 μm and 2.62 μm, respectively (Fig. S3 and S4†). However, the U-CuMgAl(NO_3)-LDH shows an enhanced sheet thickness of 0.24 μm (Fig. S4†) relative to U-CuMgAl(CO_3)-LDH (0.18 μm; Fig. S3†). The significant lattice expansion of LDH phase results from the ion exchange of interlayer CO_3^{2-} by NO_3^-. In the case CuMgAl-LDH@mSiO_2 sample, it displays irregular sheet morphology with a large lateral size distribution (Fig. 2C: 1–2 μm). Furthermore, the sheet thickness is 5.3 nm (Fig. S5†), which is far less than that of the LDH precursor. The samples of S-CuMgAl-LDH-80, S-CuMgAl-LDH-100 and S-CuMgAl-LDH-120 (Fig. 2D–F) show round-like particles, whose mean particle size increases gradually from 24.0 nm to 30.9 nm and then to 36.2 nm with the increase of crystallization temperature (Fig. S6–S8†). In particular, the average height in the *C*-axis increases from 6.1 nm (S-CuMgAl-LDH-80, Fig. S6†) to 7.0 nm (S-CuMgAl-LDH-100, Fig. S7†) and finally to 8.3 nm (S-CuMgAl-LDH-120, Fig. S8†).

Transmission electron microscopy (TEM) images further illustrate a hexagonal plate-like morphology of U-CuMgAl(CO_3)-LDH (Fig. 3A) and U-CuMgAl(NO_3)-LDH (Fig. 3B) with mean particle size of 2.58 μm (Fig. S9†) and 2.53 μm (Fig. S10†), respectively, which are consistent with the results of SEM images. The sample of CuMgAl-LDH@mSiO_2 shows a thin layer on average thickness of 5.2 nm (Fig. 3C and S11†). The LDH

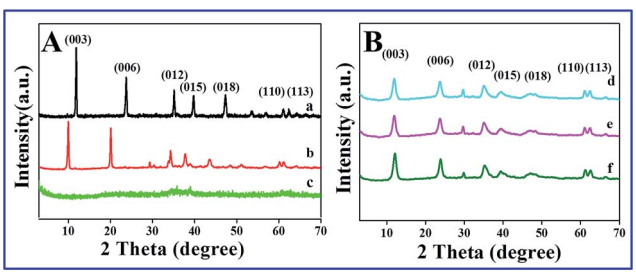

Fig. 1 (A) XRD patterns of (a) U-CuMgAl(CO_3)-LDH, (b) U-CuMgAl(NO_3)-LDH, (c) CuMgAl-LDH@mSiO_2; (B) XRD patterns of (d) S-CuMgAl-LDH-80, (e) S-CuMgAl-LDH-100, (f) S-CuMgAl-LDH-120.

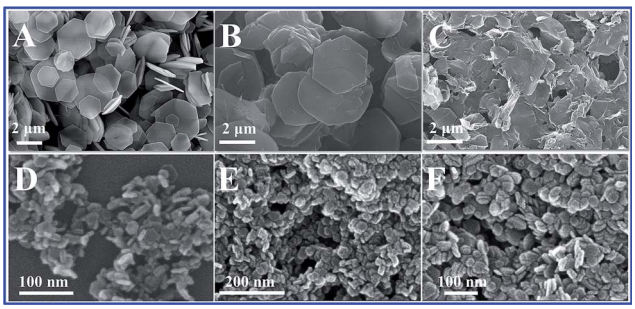

Fig. 2 SEM images of (A) U-CuMgAl(CO_3)-LDH, (B) U-CuMgAl(NO_3)-LDH, (C) CuMgAl-LDH@mSiO_2, (D) S-CuMgAl-LDH-80, (E) S-CuMgAl-LDH-100, (F) S-CuMgAl-LDH-120.

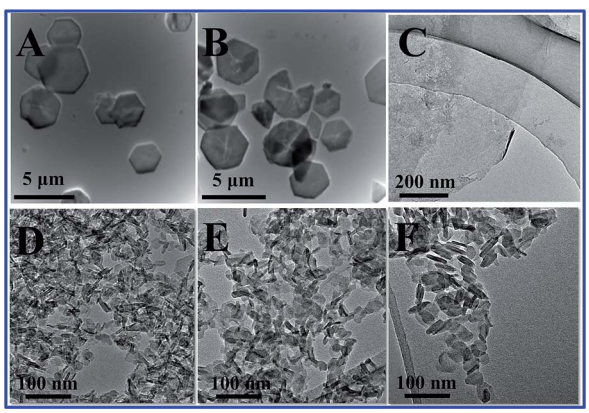

Fig. 3 TEM images of (A) U-CuMgAl(CO_3)-LDH, (B) U-CuMgAl(NO_3)-LDH. HRTEM images of (C) CuMgAl-LDH@mSiO_2, (D) S-CuMgAl-LDH-80, (E) S-CuMgAl-LDH-100 and (F) S-CuMgAl-LDH-120.

sheets are completely separated by SiO_2 coating, which is beneficial for a high exposure of active Cu^{2+} in the host layers. For the three control samples with plate-like morphology, the lateral size increases from 23.1 nm to 29.4 nm and then to 35.5 nm; while the thickness enhances gradually from 6.1 nm to 7.3 nm and finally to 8.5 nm (Fig. 3D–F and S12–S14†) with the increase of crystallization temperature. This is approximately in accordance with the SEM results (Fig. 2).

The specific surface area and pore-size distribution are two key factors for the Cu-based catalyst materials in hydroxylation applications, which were studied by N_2 adsorption/desorption isotherms and porosity measurements in this work. The U-CuMgAl(CO_3)-LDH and U-CuMgAl(NO_3)-LDH samples (Fig. 4A, curve a and b) show rather insignificant N_2-adsorption within the whole test pressure, indicating the absence of pore structure. The specific surface areas are low, which are 17.1 and 17.3 $m^2\ g^{-1}$, respectively (Table S1†). The three control samples (S-CuMgAl-LDH) display a typical IV isotherm with a H4-type hysteresis loop ($P/P_0 > 0.4$). Their specific surface areas show a decrease trend with the enhanced crystallization temperature: from 111.8 $m^2\ g^{-1}$ (S-CuMgAl-LDH-80) to 89.8 $m^2\ g^{-1}$ (S-CuMgAl-LDH-100) and finally to 75.5 $m^2\ g^{-1}$ (S-CuMgAl-LDH-120) (Fig. 4B and Table S1†). However, the average pore diameter increases from 9.9 nm (S-CuMgAl-LDH-80) to 10.5 nm (S-CuMgAl-LDH-100) and then to 15.9 nm (S-CuMgAl-LDH-120) with the enhancement of crystallization temperature (Fig. 4B and Table S1†). The results show that the mesoporous are mainly formed by the stacking of LDH nanoparticles (Fig. 4B). In contrast, the CuMgAl-LDH@mSiO_2 sample exhibits the IV isotherm with a H3-type hysteresis loop ($P/P_0 > 0.4$) (Fig. 4A, curve c). A pore-size distribution centered at 4.0 nm (pore volume: 0.461 $cm^3\ g^{-1}$) and a broad pore distribution in the range 6.0–12.0 nm are observed, indicating the existence of multilevel mesoporous structure for CuMgAl-LDH@mSiO_2 (Table S1†). Moreover, the nanosheets sample shows the largest specific surface area (Table S1: 244.3 $m^2\ g^{-1}$†) among these LDH samples.

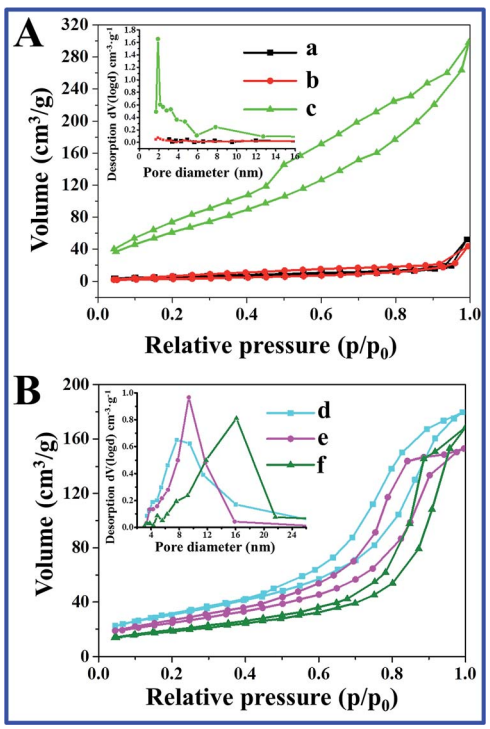

Fig. 4 (A) N_2 sorption isotherms and pore size distribution (inset) of (a) U-CuMgAl(CO_3)-LDH, (b) U-CuMgAl(NO_3)-LDH and (c) CuMgAl-LDH@mSiO_2. (B) N_2 sorption isotherms and pore size distribution (inset) of (d) S-CuMgAl-LDH-80, (e) S-CuMgAl-LDH-100, (f) S-CuMgAl-LDH-120.

3.2 Catalytic evaluation over phenol hydroxylation

Table 1 summarizes the catalytic performances in phenol hydroxylation with hydrogen peroxide over the target catalyst (CuMgAl-LDH@mSiO_2) and the control samples (S-CuMgAl-LDH and U-CuMgAl-LDH). For this catalytic reaction, a higher molar ratio of H_2O_2/phenol commonly leads to a higher phenol conversion but a lower efficiency of peroxide.[28–30] Taking into account the commercial application, it is important to improve the conversion of reactant (especially the efficiency of H_2O_2).[28–30] In this work, the efficiency of H_2O_2 is defined as the molar ratio between the consumed H_2O_2 in the formation of products and the totally added H_2O_2. To further evaluate the catalytic performance of these Cu-based catalysts, the normalized activity is calculated based on the mole of converted phenol by per mole of Cu species in the catalyst. For all of these catalysts, hydroquinone (HQ) and catechol (CAT) are obtained as major products. The selectivity of principal product over all these catalysts is above 95%, which is to our knowledge extraordinary high among Cu-based catalysts in phenol hydroxylation (Table S2†). Interestingly, the molar ratio of HQ/CAT ranges in a limited region (about 1.5–1.7), which indicates the same active site on the surface of these LDH catalysts. As shown in Table 1, the U-CuMgAl(CO_3)-LDH and U-CuMgAl(NO_3)-LDH display a low level of phenol conversion (22.7 and 23.4%), H_2O_2 efficiency (45.4 and 46.8%) and normalized activity (32.8 and 33.8 mol phenol/mol Cu^{2+}), which is due to the low specific surface area. For the three samples of S-CuMgAl-LDH (S-CuMgAl-LDH-80, S-CuMgAl-LDH-100 and S-CuMgAl-LDH-120), a significant enhancement in phenol conversion, H_2O_2 efficiency and normalized activity are observed. Moreover, the H_2O_2 efficiency increases from 60.0 to 71.8% and normalized activity increase from 29.5 to 37.5 mol phenol/mol Cu^{2+} with the decrease of crystallization temperature, which shows a specific surface area-dependant activity.

The target catalyst (CuMgAl-LDH@mSiO_2) displays the highest phenol conversion (45.6%) among the as-prepared CuMgAl-LDH samples under the same reaction conditions. The normalized activity over CuMgAl-LDH@mSiO_2 is surprisingly high (330.8 mol phenol/mol Cu^{2+}), almost ten times that of U-CuMgAl(CO_3)-LDH (32.8 mol phenol/mol Cu^{2+}) and nine times that of S-CuMgAl-LDH-80 (37.5 mol phenol/mol Cu^{2+}). Furthermore, the efficiency of H_2O_2 over CuMgAl-LDH@mSiO_2 gives the largest value (91.2%) in this work, which is also superior to previously reported ones under identical conditions to our knowledge (Tables 1 and S2†). Moreover, the catalytic

Table 1 Catalytic performances of LDH catalysts toward phenol hydroxylation[a]

Catalysts	S_{BET} (m^2 g^{-1})	Cu[b] (w%)	X_{ph}[c] (%)	S_{CAT}[c] (%)	S_{HQ}[c] (%)	S_{BQ}[c] (%)	S_{CAT+HQ}[c] (%)	R[d]	H_2O_2 eff.[e]	Normalized activity[f]
S-CuMgAl-LDH-80	111.8	6.8	35.9	60.2	35.7	4.1	95.9	1.7	71.8	37.5
S-CuMgAl-LDH-100	89.8	6.5	31.1	60.7	35.5	3.9	96.1	1.7	62.2	31.3
S-CuMgAl-LDH-120	75.5	7.2	30.0	60.2	35.6	4.2	95.8	1.7	60.0	29.5
U-CuMgAl(CO_3)-LDH	17.1	4.1	22.7	58.1	37.9	3.9	96.1	1.5	45.4	32.8
U-CuMgAl(NO_3)-LDH	17.3	4.0	23.4	59.2	36.3	3.9	95.5	1.5	46.8	33.8
CuMgAl-LDH@mSiO_2	244.3	0.93	45.6	60.7	36.6	2.7	97.3	1.6	91.2	330.8

[a] Reaction conditions: catalyst 100 mg, phenol 1 g, H_2O 10 ml, phenol : H_2O_2 (30% mass) = 2 : 1 (mole), reaction temperature 65 °C, reaction pressure 1 atm, reaction time 1 h. [b] The copper loading based on ICP. [c] Conv. = conversion of phenol; S_{CAT} and S_{HQ} denote the selectivity to catechol and hydroquinone, respectively; S_{CAT+HQ} means the selectivity to catechol and hydroquinone. [d] R represents the molar ratio of catechol to hydroquinone. [e] H_2O_2 efficiency% = 100 × (H_2O_2 consumed in the formation of products, mol)/(total H_2O_2 added, mol). [f] Normalized activity (mol phenol/mol Cu^{2+}) represents the converted phenol by per mole of copper.

performances of CuMgAl-LDH@mSiO_2 with various molar ratios of phenol : H_2O_2 are shown in Table S2† (from 5 : 1 to 1 : 1). The conversion of phenol and normalized activity enhance monotonically with the increase of H_2O_2 amount, but the efficiency of H_2O_2 decreases accordingly. Taking into account both the phenol conversion and H_2O_2 efficiency, a moderate molar ratio of phenol : H_2O_2 (2 : 1) is chosen. In addition, the CuMgAl-LDH@mSiO_2 catalyst exhibits a good reusability: both activity and selectivity toward principal product remain almost unchanged in five recycles (Fig. 5). SEM images further reveal that the particle size and morphology of the used catalyst are maintained (Fig. S15†), demonstrating its stability and recyclability. The excellent catalytic performance of CuMgAl-LDH@mSiO_2 can be ascribed to its unique structure. The CuMgAl-LDH nanosheet is coated with a layer of SiO_2 during the delamination process of U-CuMgAl(NO_3)-LDH. The delamination of bulk LDH material results in a largely enhanced specific surface area and exposed active sites, which gives rise to an improved catalytic activity toward phenol hydroxylation. In addition, the porous SiO_2 coating prevents the aggregation of LDH nanosheets without obvious influence on the mass diffusion. These features account for the excellent normalized activity and peroxide efficiency over the CuMgAl-LDH@mSiO_2 catalyst, in comparison with other heterogeneous bulk catalysts (Tables 1 and S2†).

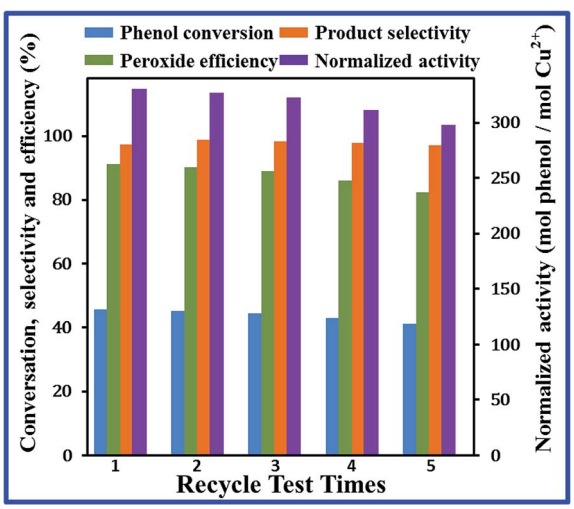

Fig. 5 Catalytic performances of the CuMgAl-LDH@mSiO_2 catalyst toward phenol hydroxylation in five consecutive recycles. The reaction conditions are the same in Table 1.

4. Conclusions

In summary, a series of CuMgAl-LDH samples were prepared to obtain different particle sizes of catalyst toward phenol hydroxylation. The resulting nanosheets catalyst (CuMgAl-LDH@mSiO_2) exhibits remarkably enhanced catalytic activity with a phenol conversion of 45.6%, selectivity of 97.3%, H_2O_2 efficiency of 91.1% and normalized activity of 330.8 mol phenol/mol Cu^{2+}, which is superior to previously reported Cu-based catalysts. In addition, a satisfactory stability and recyclability are demonstrated. This work provides a facile method for the preparation of a Cu-containing LDH catalyst with high dispersion, which serves as a promising candidate in phenol hydroxylation. It is expected that this strategy can be extended to the synthesis of other layered heterogeneous catalysts in related field.

Acknowledgements

This work was supported by the 973 Program (Grant No. 2014CB932104), the National Natural Science Foundation of China (NSFC) and the Fundamental Research Funds for the Central Universities (YS1406).

Notes and references

1 J. H. Clark, *Green Chem.*, 1999, **1**, 1–8.
2 P. M. Hudnall, in *Ullmann's Encyclopedia of Industrial Chemistry*, Wiley-VCH Verlag GmbH & Co. KGaA, 2000.
3 U. Wilkenhoener, G. Langhendries, F. van Laar, G. V. Baron, D. W. Gammon, P. A. Jacobs and E. van Steen, *J. Catal.*, 2001, **203**, 201–212.
4 J. Wang, J. N. Park, X. Y. Wei and C. W. Lee, *Chem. Commun.*, 2003, 628–629.
5 J. Sun, X. Meng, Y. Shi, R. Wang, S. Feng, D. Jiang, R. Xu and F. S. Xiao, *J. Catal.*, 2000, **193**, 199–206.

6 J. Varagnat, *Ind. Eng. Chem. Prod. Res. Dev.*, 1976, **15**, 212–215.
7 M. B. Hocking and D. J. Intihar, *J. Chem. Technol. Biotechnol., Chem. Technol.*, 1985, **35**, 365–381.
8 M. R. Maurya, S. J. J. Titinchi, S. Chand and I. M. Mishra, *J. Mol. Catal. A: Chem.*, 2002, **180**, 201–210.
9 X. Zhang, Y. Li, G. Li and C. Hu, *RSC Adv.*, 2015, **5**, 4984–4992.
10 J. Sun, X. Meng, Y. Shi, R. Wang, S. Feng, D. Jiang, R. Xu and F. Xiao, *J. Catal.*, 2000, **193**, 199–206.
11 S. He, S. Zhang, J. Lu, Y. Zhao, J. Ma, M. Wei, D. G. Evans and X. Duan, *Chem. Commun.*, 2011, **47**, 10797–10799.
12 Q. Wang and D. O'Hare, *Chem. Rev.*, 2012, **112**, 4124–4155.
13 G. L. Fan, F. Li, D. G. Evans and X. Duan, *Chem. Soc. Rev.*, 2014, **43**, 7040–7066.
14 L. Li, R. Ma, Y. Ebina, K. Fukuda, K. Takada and T. Sasaki, *J. Am. Chem. Soc.*, 2007, **129**, 8000–8007.
15 E. Coronado, C. Martí-Gastaldo, A. E. Navarro-Moratalla, S. J. B. Ribera and P. J. Baker, *Nat. Chem.*, 2010, **2**, 1031–1036.
16 C. Li, R. Liang, R. Tian, S. Guan, D. Yan, J. Luo, M. Wei, D. G. Evans and X. Duan, *RSC Adv.*, 2016, **6**, 16608–16614.
17 S. Kannan, A. Dubey and H. Knozinger, *J. Catal.*, 2005, **231**, 381–392.
18 C. A. Antonyraj, M. Gandhi and S. Kannan, *Ind. Eng. Chem. Res.*, 2010, **49**, 6020–6026.
19 H. Zhang, G. Zhang, X. Bi and X. Chen, *J. Mater. Chem. A*, 2013, **1**, 5934–5942.
20 T. Baskaran, J. Christopher and A. Sakthivel, *RSC Adv.*, 2015, **5**, 98853–98875.
21 Z. Liu, R. Ma, Y. Ebina, N. Iyi, K. Takada and T. Sasaki, *Langmuir*, 2007, **23**, 861–867.
22 D. Yan, J. Lu, M. Wei, S. Qin, L. Chen, S. Zhang, D. G. Evans and X. Duan, *Adv. Funct. Mater.*, 2011, **21**, 2497–2505.
23 G. Wang, S. Xu, C. Xia, D. Yan, Y. Lin and M. Wei, *RSC Adv.*, 2015, **5**, 23708–23714.
24 O. V. Kharissova, B. I. Kharisov, V. M. Jiménezpérez, B. M. Flores and U. O. Méndez, *RSC Adv.*, 2013, **3**, 22648–22682.
25 Y. Zhao, F. Li, R. Zhang, D. G. Evans and X. Duan, *Chem. Mater.*, 2002, **14**, 4286–4291.
26 T. L. P. Galvao, C. S. Neves, A. P. F. Caetano, F. Maia, D. Mata, E. Malheiro, M. J. Ferreira, A. C. Bastos, A. N. Salak, J. R. B. Gomes, J. Tedim and M. G. S. Ferreira, *J. Colloid Interface Sci.*, 2016, **468**, 86–94.
27 J. Z. Xie, K. Zhang, J. F. Wu, G. F. Ren, H. Y. Chen and J. Xu, *Appl. Clay Sci.*, 2016, **126**, 72–80.
28 J. Wang, J.-N. Park, H.-C. Jeong, K.-S. Choi, X.-Y. Wei, S.-I. Hong and C. W. Lee, *Energy Fuels*, 2004, **18**, 470–476.
29 G. Yang, X. Hu, Y. Wu, C. Liu and Z. Zhang, *Catal. Commun.*, 2012, **26**, 132–135.
30 M. Jin, R. Yang, M. Zhao, G. Li and C. Hu, *Ind. Eng. Chem. Res.*, 2014, **53**, 2932–2939.